NNLO QCD corrections to weak boson fusion Higgs boson production in the $H \to b\bar{b}$ and $H \to WW^* \to 4l$ decay channels

Konstantin Asteriadis,[1,*] Fabrizio Caola,[2,†] Kirill Melnikov,[3,‡] and Raoul Röntsch[4,5,§]

[1] *High Energy Theory Group, Physics Department,*
Brookhaven National Laboratory, Upton, NY 11973, USA

[2] *Rudolf Peierls Centre for Theoretical Physics, Clarendon Laboratory, Parks*
Road, Oxford OX1 3PU, UK and Wadham College, Oxford OX1 3PN, UK

[3] *Institute for Theoretical Particle Physics, KIT, Karlsruhe, Germany*

[4] *Theoretical Physics Department, CERN, 1211 Geneva 23, Switzerland*

[5] *Tif Lab, Dipartimento di Fisica, Università di Milano and*
INFN, Sezione di Milano, Via Celoria 16, I-20133 Milano, Italy

Abstract

We compute the next-to-next-to-leading order QCD corrections to Higgs boson production in weak boson fusion followed by its decay to a $b\bar{b}$ pair or to a pair of leptonically-decaying W bosons. Our calculation allows us to compute realistic fiducial cross sections and assess the impact of fiducial cuts applied to the Higgs boson decay products on the magnitude of QCD radiative corrections in weak boson fusion.

* Electronic address: kasteriad@bnl.gov

† Electronic address: fabrizio.caola@physics.ox.ac.uk

‡ Electronic address: kirill.melnikov@kit.edu

§ Electronic address: raoul.rontsch@cern.ch

I. INTRODUCTION

Precision studies of Higgs boson properties are central to the physics program of the Run III and high-luminosity phases of the LHC. Currently, all major Higgs production cross sections and decay rates are known experimentally to a precision of about twenty percent or better [1, 2]. These measurements are used to determine Higgs couplings to a variety of elementary particles, confirming that the Higgs boson profile emerging from the LHC data is very consistent with expectations based on the Standard Model.

Further exploration of the Higgs boson will lead to an even better understanding of its properties. Central to this endeavor is the overarching goal of the LHC experiments to determine Higgs couplings with a few percent precision, allowing for a detailed exploration of the structure of the Standard Model. To facilitate this progress, precise theoretical predictions for all the major Higgs boson production and decay processes are required. Such predictions must, on the one hand, account for higher order radiative corrections and, on the other hand, describe observable final states in as much detail as possible. The recent past has seen impressive progress in the development of high-quality theoretical predictions for Higgs production and decay processes at colliders, see e.g. Ref. [3] for a review.

In this paper, we focus on Higgs boson production in weak boson fusion (WBF). Being the channel with the next-to-largest cross section at the LHC, it allows for detailed studies of the structure of the Higgs sector. Indeed, phenomenologically, this channel is important for a direct determination of the Higgs couplings to the electroweak bosons, for investigating the CP-structure of the Higgs boson [4–6] and for studies of Higgs decays into invisible particles [7, 8].

Higgs production in WBF has been investigated by both ATLAS and CMS using a number of Higgs decay modes. One finds $\mu_{\text{VBF}} = 1.21 \pm 0.18$ (stat.) ± 0.15 (syst.) (ATLAS) [1] and $\mu_{\text{VBF}} = 0.73 \pm 0.23$ (stat.) ± 0.16 (syst.) (CMS) [2] for the signal strength in this channel relative to the Standard Model expectations. These studies are supported by the development of sophisticated theoretical tools that allow accurate descriptions of Higgs boson production in WBF.[1]

----

[1] For a review of the state-of-the-art predictions for this channel, see Ref. [9]. Recent phenomenological studies are summarized in Ref. [10].

At leading order, WBF production involves the two incoming partons emitting space-like Z's and W's that fuse into the Higgs boson. This gives WBF events a characteristic signature of two forward jets in opposite hemispheres, and means that WBF can be viewed as a double deep inelastic scattering (DIS) process [11]. At next-to-leading order (NLO) in QCD, color conservation forbids interactions that connect the two quark lines, so that the double-DIS picture of WBF is still exact.[2] As a consequence of this simplification, NLO QCD corrections to WBF were computed early on and have been known for almost twenty years by now [14].

At next-to-next-to-leading order (NNLO), QCD interactions between two quark lines become possible, so that the double-DIS picture of WBF is no longer exact. However, the double-DIS and the so-called non-factorizable contributions are separately finite and gauge-invariant and, therefore, can be studied independently. Theoretical predictions for the double-DIS contributions are very advanced. In this approximation, the total cross section is known to NNLO [15] and N³LO [16] in QCD, while fully differential results – which are crucial for a reliable modeling of the WBF process – are available at NNLO QCD [17, 18].

On the contrary, the non-factorizable contributions are much less understood since no exact results exist in this case. Recently, the leading non-factorizable QCD corrections that appear at NNLO QCD have been estimated [19]. Although non-factorizable corrections are known to be color-suppressed [15], it was explicitly shown in Ref. [19] that they get enhanced by additional factors of π^2 leading to a partial compensation of the color suppression factor. A comprehensive discussion of phenomenological aspects of non-factorizable corrections can be found in Ref. [20].

All the NNLO calculations mentioned above do not include the decay of the Higgs boson and, therefore, cannot describe realistic final states in WBF. Since the Higgs boson is a narrow scalar particle, its production and decay stages are completely separated. Hence, the inclusion of Higgs decays is, in principle, straightforward. However, in practice this turns out to be non-trivial for fully differential NNLO QCD calculations. One may naively think of performing a NNLO calculation with a stable Higgs boson, storing events with the relevant kinematic information and including the Higgs decays in a second stage. In fact, this strategy is routinely employed in complex NLO calculations. However, the number

---

[2] This statement does not hold for interference contributions to the $qq \to Hqq$ amplitude squared. However, these contributions are known to be tiny when WBF cuts are applied [10, 12, 13].

of events needed for a NNLO calculation of the WBF type is extremely high, making this approach impractical.[3] As the result, NNLO QCD predictions for Higgs production in WBF including Higgs decays are currently not available. This limitation is important as kinematic cuts applied to the decay products of the Higgs boson may alter the impact of NNLO QCD corrections. Even if such modifications turn out to be small, they may still be relevant at NNLO QCD accuracy, given that both the size of the NNLO corrections and the residual scale uncertainty for Higgs production in WBF are at the level of a few percent.

In this paper, we make a first step towards NNLO QCD predictions for Higgs production in WBF with realistic final states. Similarly to the earlier calculations of Ref. [17, 18] we only consider the double-DIS contributions but we include Higgs decays in our computation. We consider two representative cases – Higgs decays to a pair of b quarks and Higgs decays to two W bosons which decay leptonically in turn. Since both of these final states have large branching ratios, they have been extensively studied by the ATLAS [22, 23] and CMS [24, 25] collaborations. Our calculations allow us to investigate the impact of kinematic constraints applied to final state particles on the magnitude of QCD corrections to fiducial cross sections and kinematic distributions in the presence of realistic selection criteria.

In principle, a proper modeling of Higgs-boson decays to b pairs would require the inclusion of b-quark mass effects (so that a realistic jet algorithm can be adopted) and higher-order QCD radiative corrections. Although all the required ingredients exist [26, 27], combining them into an efficiently working computer program is a major undertaking if NNLO QCD precision is desired. For this reason, in this paper we restrict ourselves to Higgs decays into massless $b\bar{b}$ pairs at leading order in QCD.[4] This is the first non-trivial step towards a NNLO-accurate description of the weak boson fusion process with Higgs decays into $b\bar{b}$ pairs.

On a technical side, we note that the previous NNLO QCD calculations of Refs. [17, 18] were performed using the projection-to-Born [17] and antenna subtraction [28] methods, respectively, to regulate infrared singularities. For the computation described in this paper we employ the nested soft-collinear subtraction scheme [29], using analytic formulas for the integrated subtraction terms derived in Ref. [30]. This is the first phenomenological

---

[3] A recent summary on progress in this direction was given in Ref. [21].

[4] Of course, for leading order $H \to b\bar{b}$ decay dealing with massless, as opposed to massive, b-quarks does not change the complexity of the calculation.

application of this method to a complex LHC process involving final-state jets, marking an important step in its development.

The paper is organized as follows. In Section II we briefly summarize some technical aspects of the calculation of NNLO QCD corrections to Higgs production in WBF within the nested soft-collinear subtraction scheme. In Section III we apply our computation to perform NNLO QCD phenomenological studies at the 13 TeV LHC. We first present results for stable Higgs boson (Section III A), showing perfect agreement with earlier calculations. We then discuss the $H \to b\bar{b}$ (Section III B) and $H \to WW^* \to \ell^- \bar{\nu} \ell^+ \nu$ (Section III C) cases, focusing on the interplay of fiducial cuts on the final state particles and NNLO QCD corrections. We conclude in Section IV.

II. NESTED SOFT-COLLINEAR SUBTRACTION CALCULATION OF NNLO QCD CORRECTIONS TO WEAK BOSON FUSION

In this section we summarize the technical aspects of the calculation including a brief discussion of the nested soft-collinear subtraction scheme [29] and an explanation of how we apply it to the computation of factorizable NNLO QCD corrections to Higgs boson production in weak boson fusion. We note that this section is not meant to provide a self-contained discussion of the nested soft-collinear subtraction scheme. We refer the interested reader to Refs. [29, 30] for a thorough explanation of all the relevant details.

It is well-known that fully-differential QCD computations suffer from infra-red and collinear singularities that appear differently in virtual and real corrections. In the case of virtual corrections, these singularities manifest themselves as explicit poles in the dimensional regularization parameter. The universal structure of these singularities has been known for a long time [31, 32].

The situation with the real-emission contributions is quite different. Indeed, in this case infra-red and collinear singularities arise from the integration over the phase space of final state partons that appear at higher orders in QCD, in addition to the particles present in the Born process. However, if one's goal is a fully-differential computation valid for arbitrary infra-red safe observables, such integration is not possible both in theory and in practice.

The solution to this problem involves isolating phase-space regions that contribute to infrared and collinear singularities. The standard ways for dealing with them are the so-called slicing and subtraction methods, which regulate the singular regions of the phase space by adding and subtracting cleverly-constructed counterterms. In the past decade, a large number of such schemes has been developed for NNLO QCD computations [17, 28, 33–38]. In this paper, we employ the so-called nested soft-collinear subtraction scheme [29].

The idea behind this scheme is an iterative construction of subtraction counterterms, starting from the soft ones. The soft subtraction terms are given by universal eikonal currents multiplied by amplitudes with lower multiplicities. For the non-trivial case of double-unresolved contributions, they were integrated over the phase space of unresolved partons in Ref. [39] using the universal double-soft limits of scattering amplitudes computed in Ref. [40].

The collinear regularization procedure is then applied to soft-regulated matrix elements. In analogy with the FKS construction at NLO [41], different collinear directions are separated with the help of suitably-constructed partitions of unity. For triple-collinear configurations, different strongly-ordered collinear limits can be approached in different ways; as the result, an angular ordering is employed to uniquely define them. This can be achieved by introducing a particular phase-space parametrization for the two unresolved partons [33] that allows for a natural separation of various collinear configurations. Among the various collinear subtraction terms that need to be considered, the triple-collinear ones are the most complicated; they were integrated over the phase space of the unresolved partons in Ref. [42].

Apart from the subtraction terms for double-unresolved configurations, the remaining contributions to the subtraction counterterms include various soft and collinear limits that either involve kinematic configurations that are significantly simpler than the double-unresolved ones or correspond to soft-collinear configurations which are relatively easy to deal with.

Finally, we note that the subtraction terms and their integrals over unresolved phase spaces involve *universal* functions that appear in soft and collinear limits of matrix elements; hence, they are fully determined by the number, types and color charges of external particles, and are independent of the matrix elements of hard processes. Since factorizable corrections to weak boson fusion process involve a t-channel momentum transfer by a colorless vector boson, they are topologically similar to QCD corrections in deep inelastic scattering (DIS), as mentioned previously. The calculation of integrated subtraction terms for DIS has been
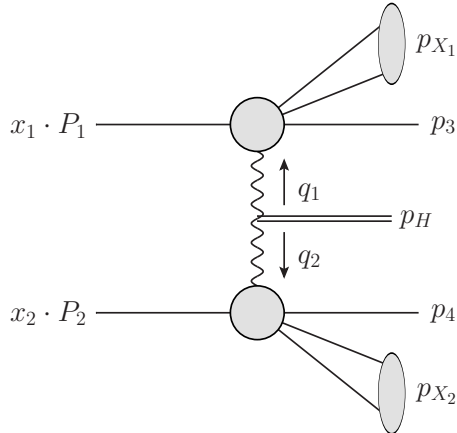
Figure 1. Conventions used for the generation of the phase space to compute factorizable contributions to Higgs production in WBF. Momenta p_{X_1} and p_{X_2} are combined momenta of all additional (massless) partons radiated from the upper or the lower line, respectively

performed in the context of the nested soft-collinear subtraction scheme in Ref. [30]. We can then use results obtained in that reference for the WBF case as well. We refer the reader to Ref. [30] for further details regarding the subtraction scheme.

It is well-known that one of the challenging issues pertinent to the computation of higher order QCD corrections to weak boson fusion is the phase-space parametrization. Such a parametrization should, on the one hand, lead to an efficient sampling of the phase space and, therefore, to an efficient Monte-Carlo integration and, on the other hand, it should also allow for a seamless connection with the subtraction scheme. Because of this, we now briefly describe how the phase space is parametrized in our computation.

At variance with earlier applications of the nested soft-collinear subtraction scheme, we work in the laboratory frame, i.e. in the center-of-mass frame of the incoming *protons*. We consider the generic process shown in Fig. 1. We assume that particles with momenta p_3 and p_4 are "hard" and particles collectively denoted with $p_{X_{1,2}}$ can become soft and collinear to other particles. The separation into hard and soft particles either happens naturally (for example, for the NNLO subprocess $qq \to Hqq + gg$ the hard partons are the two final-state quarks while the partons that can become soft and collinear are the gluons) or it is achieved by introducing additional partition functions (as it happens in the case of several quarks in the final state). An analogous procedure was carried out for computing the NNLO QCD corrections to DIS [30] and we make use of it in the current calculation.

Using the notation in Fig. 1, we schematically write the weak boson fusion cross sections in the following way

$$\sigma = \mathcal{N} \int_0^1 \frac{dx_1 dx_2 f_1(x_1) f_2(x_2)}{2 s_{\text{had}} x_1 x_2} \int [dp_3][dp_4][dp_{X_1}][dp_{X_2}][dp_H]$$
$$\times (2\pi)^d \delta^{(d)} \left(P_i - P_f \right) \left| \mathcal{M}(x_1 P_1, x_2 P_2 \, ; \, p_3, p_{X_1}, p_4, p_{X_2}, p_H) \right|^2 , \tag{1}$$

where $\mathcal{N}$ is the (possible) symmetry and averaging factor, $P_{1,2}$ are the protons' momenta, $P_i = x_1 P_1 + x_2 P_2$, $P_f = p_3 + p_4 + p_{X_1} + p_{X_2} + p_H$ and $s_{\text{had}} = (P_1 + P_2)^2$ is the *hadronic* center-of-mass energy. Also, $f_{1,2}$ are parton distribution functions, $\mathcal{M}$ is the relevant matrix element that depends on the momenta of initial- and final-state particles and $[dp]$ is the phase-space element for a particle or a collection of particles with momenta p. More precisely, we define

$$[dp_i] = \frac{d^{d-1} p_i}{(2\pi)^{d-1} 2 E_i}, \tag{2}$$

for a single particle and

$$[dp_{X_i}] = \prod_{i \in X_i} \frac{d^{d-1} p_i}{(2\pi)^{d-1} 2 E_i}, \tag{3}$$

for several particles. Finally, we set $[dp_{X_i}] = 1$ if X_i does not contain any particle.

To proceed further, we introduce two auxiliary momenta $q_{1,2}$ defined as follows (see Fig. 1)

$$q_1 = p_3 + p_{X_1} - x_1 P_1 , \qquad q_2 = p_4 + p_{X_2} - x_2 P_2 . \tag{4}$$

We then insert unity into the phase-space integrand and write

$$1 = \int_0^{\mu_{\text{max}}^2} d\mu_i^2 \; \delta(\mu_i^2 + q_i^2) , \tag{5}$$

for $i = 1, 2$. We note that the relative sign between μ_i^2 and q_i^2 in the argument of the delta-function is due to the fact that the momenta $q_{1,2}^2$ are space-like. In the above formula μ_{max}^2 is an arbitrary quantity with the dimension of energy squared. We note that μ_{max} should be large enough to accommodate all the relevant values of $|q_{1,2}^2|$; we take it to be $\mu_{\text{max}}^2 = s_{\text{had}} - m_H^2$, where m_H is the mass of the Higgs boson.

The benefit of having the delta-function in Eq. (5) to appear in the WBF phase space follows from the fact that its argument is linear in x_i, $i = 1, 2$. Indeed, using explicit expressions

for $q_{1,2}$ and the fact that $P_i^2 = 0$, we find

$$\begin{aligned}
\delta(\mu_i^2 + q_i^2) &= \delta(\mu_i^2 + (p_{3,4} + p_{X_i} - x_i P_i)^2) \\
&= \delta(\mu_i^2 + (p_{3,4} + p_{X_i})^2 - 2x_i(p_{3,4} + p_{X_i})P_i) \\
&= \frac{1}{|2(p_{3,4} + p_{X_i})P_i|} \, \delta\left(\frac{\mu_i^2 + (p_{3,4} + p_{X_i})^2}{2(p_{3,4} + p_{X_i})P_i} - x_i\right).
\end{aligned}$$

(6)

We can then use these expressions to integrate over $x_{1,2}$ in Eq. (1). We find

$$\begin{aligned}
\sigma = \int\limits_0^{\mu_{\text{max}}^2} \mathrm{d}\mu_1^2 \, \mathrm{d}\mu_2^2 \int \frac{[\mathrm{d}p_3][\mathrm{d}p_4][\mathrm{d}p_{X_1}][\mathrm{d}p_{X_2}][\mathrm{d}p_H]}{2s_{\text{had}}x_1^* x_2^*} \frac{f_1(x_1^*) f_2(x_2^*)}{|2(p_3 + p_{X_1})P_1||2(p_4 + p_{X_2})P_2|} \\
\times (2\pi)^d \delta^{(d)}\left(P_i^* - P_f\right) |\mathcal{M}(x_1^* P_1, x_2^* P_2 \, ; \, p_3, p_{X_1}, p_4, p_{X_2}, p_H)|^2 ,
\end{aligned}$$

(7)

where $P_i^* = x_1^* P_1 + x_2^* P_2$ and

$$x_i^* = \frac{\mu_i^2 + (p_{3,4} + p_{X_i})^2}{2(p_{3,4} + p_{X_i})P_i}, \qquad i = 1, 2.$$

(8)

We require, of course, that $x_i^* \in [0, 1]$; if this is not the case, the corresponding kinematic points are rejected.

We remove the delta-function in Eq. (7) by integrating over the four-momentum p_H of the Higgs boson. We use

$$\begin{aligned}
[\mathrm{d}p_H] \, (2\pi)^d \delta^{(d)}(x_1 P_1 + x_2 P_2 - p_3 - p_4 - p_{X_1} - p_{X_2} - p_H) \\
= 2\pi \, \delta\left((q_1 + q_2)^2 - m_H^2\right) = 2\pi \, \delta\left(-\mu_1^2 - \mu_2^2 + 2(q_1 q_2) - m_H^2\right),
\end{aligned}$$

(9)

and remove this last delta-function by integrating over μ_2^2. We should, however, account for the fact that q_2 depends on x_2^* which, in turn, depends on μ_2^2 implicitly.

Integrating over μ_2^2, we find

$$\begin{aligned}
\sigma = \int\limits_0^{\mu_{\text{max}}^2} \mathrm{d}\mu_1^2 \int [\mathrm{d}p_3][\mathrm{d}p_4][\mathrm{d}p_{X_1}][\mathrm{d}p_{X_2}] \frac{f_1(x_1^*) f_2(x_2^*)}{2s_{\text{had}} x_1^* x_2^*} \times \frac{2\pi}{|4(q_1 P_1)(p_H P_2)|} \\
\times |\mathcal{M}(x_1^* P_1, x_2^* P_2 \, ; \, p_3, p_4, \dots)|^2 ,
\end{aligned}$$

(10)

where $p_H = q_1 + q_2$ and

$$\mu_2^2 = \frac{(p_4 + p_{X_2})P_2}{(p_4 + p_{X_2} + q_1)P_2} \times \left[-m_H^2 - \mu_1^2 + \left(2(p_4 + p_{X_2})q_1 - \frac{(p_4 + p_{X_2})^2(q_1 P_2)}{(p_4 + p_{X_2})P_2}\right)\right]$$

(11)

should be used when computing x_2^* and q_2.

The expression for the cross section in Eq. (10) is general; it can be used at any order in perturbation theory and for various combinations of emissions off initial and final states. For our calculation, we will mainly need to consider the case of two emissions off the upper (lower) quark line and, consequently, no emissions off the lower (upper) quark line. Focusing on the emissions off the upper line, we set $[\mathrm{d}p_{X_2}] \to 1$ in the expression for the phase space in Eq. (10), and $p_{X_2} \to 0$ in Eq. (11). Since $p_4^2 = 0$, the expression for μ_2 simplifies to

$$\mu_2^2 = \frac{(p_4 P_2)}{(p_H P_2)} \times \left[m_H^2 + \mu_1^2 - 2(q_1 p_4) \right] . \tag{12}$$

Finally, we note that if at NLO or at NNLO additional emissions occur only at the lower line in Fig. 1, it is of course beneficial to integrate over μ_1^2, instead of μ_2^2. We do not write an explicit formula for the cross section in this case as it can simply be obtained by a trivial re-labeling of various particles in the expressions given in Eqs. (10,11).

Having derived a suitable parametrization of the weak boson fusion phase space, we will have to use it to construct both the subtraction terms and their integrated counterparts required to extract and regulate all the relevant infra-red and collinear divergences. To this end, we would like to use the results for DIS that we have derived in Ref. [30]. However, in that reference the subtraction framework was constructed in the *partonic* center-of-mass frame. Since the subtraction formalism of Ref. [29] is not manifestly boost invariant, it is not immediately obvious that one could use the results of Ref. [30] here without modifications.

To illustrate the connection between the phase space parametrization in Eq. (10) and Ref. [30], we describe how the construction of a typical subtraction term derived in Ref. [30] would proceed. For the sake of argument, we consider the emission of two gluons with momenta $p_{5,6}$ off the upper (quark) line in Fig. 1 and study the limit when p_6 is collinear to the incoming proton P_1. The operator that extracts the relevant limit from the cross section is referred to as C_{61} in Ref. [30]. In that reference, we worked at fixed x_1, x_2 and wrote the collinear subtraction term as

$$
\begin{aligned}
C_{61}\left[\sigma\right] = g_s^2 \int \frac{\mathrm{d}x_1 \mathrm{d}x_2 f(x_1) f(x_2)}{2s_{\mathrm{had}} x_1 x_2} \int \prod_{i=3}^{6} [\mathrm{d}p_i](2\pi)^d \delta^{(d)}\left(zx_1 P_1 + x_2 P_2 - p_3 - p_4 - p_5\right) \\
\times \frac{1}{(P_1 p_6)} P_{qq}(z) \frac{|\mathcal{M}(zx_1 P_1, x_2 P_2\,;\, p_3, p_4, p_5)|^2}{zx_1} ,
\end{aligned} \tag{13}
$$

where g_s is the (bare) strong coupling constant and P_{qq} is the standard (d-dimensional) LO splitting function whose precise form is irrelevant for our discussion. The variable z is related to the energy of the gluon with momentum p_6 as $E_6 = x_1 E_1 (1 - z)$, where E_1 is the energy of the incoming *proton*.

We then write

$$[\mathrm{d}p_6] = \frac{\mathrm{d}\Omega_6}{2(2\pi)^{d-1}} (x_1 E_1)^{2-2\epsilon} \mathrm{d}z (1 - z)^{1-2\epsilon}, \tag{14}$$

and use this expression in Eq. (13) to find (see Ref. [30] for details)

$$
\begin{aligned}
C_{61}[\sigma] = -[\alpha_s] \frac{\Gamma(1-\epsilon)^2}{\Gamma(1-2\epsilon)\epsilon} \int & \frac{\mathrm{d}x_1 \mathrm{d}x_2 f(x_1) f(x_2)}{2 s_{\mathrm{had}} x_1 x_2} (2 x_1 E_1)^{-2\epsilon} \int \mathrm{d}z \, (1 - z)^{-2\epsilon} P_{qq}(z) \\
& \times \int \prod_{i=3}^{5} [\mathrm{d}p_i] (2\pi)^d \delta^{(d)} (z x_1 P_1 + x_2 P_2 - p_3 - p_4 - p_5) \\
& \times \frac{|\mathcal{M}(z x_1 P_1, x_2 P_2 \, ; \, p_3, p_4, p_5)|^2}{z},
\end{aligned}
\tag{15}
$$

where we have defined $[\alpha_s] = (g_s^2 / 8\pi^2) \times (4\pi)^\epsilon / \Gamma(1 - \epsilon)$.

We now repeat the same computation using the phase-space parametrization in Eq. (10). The difference with what we just did originates from the fact that in Eq. (10) the Bjorken variables $x_{1,2}$ are not free parameters anymore but, rather, are determined from the kinematics of final state particles. Hence, when we extract the collinear limits of the cross sections, we have to act on $x_{1,2}$ as well.

Using Eq. (8), we find

$$C_{61}[x_1^*] = \bar{x}_1^* = x_1^{\mathrm{NLO}} + \frac{E_6}{E_1}, \tag{16}$$

where

$$x_1^{\mathrm{NLO}} = \frac{\mu_1^2 + (p_3 + p_5)^2}{2(p_3 + p_5)P_1}, \tag{17}$$

is the Bjorken x that one would have obtained by performing a NLO calculation with a parton p_5 in the final state. We also find that

$$C_{61}[x_2^*] = \frac{C_{61}[\mu_2^2]}{2(p_4 P_2)} \equiv x_2^{\mathrm{NLO}}, \tag{18}$$

and that the collinear limit of μ_2^2 is determined by the collinear limit of q_1 which is given by

$$q_1 \to \bar{q}_1 = p_3 + p_{X_1} - \bar{x}_1^* P_1 = p_3 + p_5 - x_1^{\mathrm{NLO}} P_1. \tag{19}$$

Again, this is the expression for the momentum transfer that one obtains in the NLO computation where an additional parton with momentum p_5 is emitted.

We can now compute the collinear limit of the cross section using the phase-space parametrization Eq. (10). We find

$$
C_{61}\left[d\sigma\right] = g_s^2 \int d\mu^2 \int [dp_3][dp_4][dp_5][dp_6] \, \frac{f_1(\bar{x}_1^*) \, f_2(\bar{x}_2^*)}{2s_{\text{had}}\bar{x}_1^*\bar{x}_2^*} \frac{2\pi}{|4(\bar{q}_1 P_1)(p_H P_2)|}
$$
$$
\times \, \delta_{\text{mom-cons}} \times \frac{1}{\bar{x}_1^*(P_1 p_6)} \times \frac{\bar{x}_1^* E_1}{\bar{x}_1^* E_1 - E_6} P_{qq}\left(\frac{\bar{x}_1^* E_1 - E_6}{\bar{x}_1^* E_1}\right) \qquad (20)
$$
$$
\times \, |\mathcal{M}([\bar{x}_1^* - E_6/E_1] \, P_1, \bar{x}_2^* P_2 \,; \, \ldots, p_5)|^2 \, ,
$$

where we have used $P_{qq}(1/z) = -P_{qq}(z)/z$ and defined

$$
\delta_{\text{mom-cons}} = (2\pi)^d \delta^{(d)}\left([\bar{x}_1^* - E_6/E_1] \, P_1 + \bar{x}_2^* P_2 - p_3 - p_4 - p_5\right). \qquad (21)
$$

The reduced matrix element squared simplifies

$$
|\mathcal{M}([\bar{x}_1^* - E_6/E_1] \, P_1, \bar{x}_2^* P_2 \,; \, \ldots, p_5)|^2 = \left|\mathcal{M}\left(x_1^{\text{NLO}} P_1, x_2^{\text{NLO}} P_2 \,; \, \ldots, p_5\right)\right|^2. \qquad (22)
$$

An analogous simplification occurs in the argument of the delta-function in Eq. (21) where we find

$$
\delta_{\text{mom-cons}} = (2\pi)^d \delta^{(d)}\left(x_1^{\text{NLO}} P_1 + x_2^{\text{NLO}} P_2 - p_3 - p_4 - p_5\right). \qquad (23)
$$

To simplify Eq. (20) further, we introduce a new variable z

$$
z = \frac{\bar{x}_1^* E_1 - E_6}{\bar{x}_1^* E_1} = \frac{x_1^{\text{NLO}}}{x_1^{\text{NLO}} + \frac{E_6}{E_1}}, \qquad (24)
$$

and express the energy of the collinear gluon through z. We find

$$
E_6 = E_1 \, x_1^{\text{NLO}} \left(\frac{1-z}{z}\right), \qquad (25)
$$

and $\bar{x}_1^* = x_1^{\text{NLO}}/z$.

As a result, the collinear limit of the cross section becomes

$$
C_{61}\left[d\sigma\right] = g_s^2 \int d\mu^2 \int \prod_{i=3}^{6}[dp_i] \, \frac{f_1(x_1^{\text{NLO}}/z) \, f_2(x_2^{\text{NLO}})}{2s_{\text{had}}x_1^{\text{NLO}}x_2^{\text{NLO}}} \frac{z^2}{x_1^{\text{NLO}}(P_1 p_6)}
$$
$$
\times \, \delta_{\text{mom-cons}} \times \frac{P_{qq}(z)}{z} \left|\mathcal{M}\left(x_1^{\text{NLO}} P_1, x_2^{\text{NLO}} P_2 \,; \, \ldots, p_5\right)\right|^2 \qquad (26)
$$
$$
\times \, \frac{2\pi}{|4(\bar{q}_1 P_1)(p_H P_2)|}.
$$

Writing

$$
[dp_6] = \frac{d\Omega_6}{2(2\pi)^{d-1}} E_6^{1-2\epsilon} dE_6 = \frac{d\Omega_6}{2(2\pi)^{d-1}} \left[\frac{E_1 x_1^{\text{NLO}}(1-z)}{z}\right]^{1-2\epsilon} \frac{E_1 x_1^{\text{NLO}} dz}{z^2}, \qquad (27)
$$

12

and using this expression in Eq. (26), we arrive at

$$
C_{61}\,[\mathrm{d}\sigma] = -[\alpha_s]\frac{\Gamma(1-\epsilon)^2}{\Gamma(1-2\epsilon)\epsilon}\int \mathrm{d}\mu^2\int\prod_{i=3}^{5}[\mathrm{d}p_i]\;\int \mathrm{d}z(1-z)^{-2\epsilon}\left(\frac{2E_1 x_1^{\mathrm{NLO}}}{z}\right)^{-2\epsilon}
$$

$$
\times\,\delta_{\mathrm{mom-cons}}\times\frac{P_{qq}(z)}{z}\frac{\left|\mathcal{M}\!\left(x_1^{\mathrm{NLO}}P_1, x_2^{\mathrm{NLO}}P_2\,;\,\ldots,p_5\right)\right|^2}{2s_{\mathrm{had}}x_1^{\mathrm{NLO}}x_2^{\mathrm{NLO}}} \tag{28}
$$

$$
\times\,f_1(x_1^{\mathrm{NLO}}/z)\;f_2(x_2^{\mathrm{NLO}})\frac{2\pi}{|4(\bar{q}_1 P_1)(p_H P_2)|}.
$$

The above equation and Eq. (15) look different. However it is easy to see that by using the phase-space parametrization of Eq. (10) in Eq. (15) and integrating over the Bjorken variables $x_{1,2}$, one obtains Eq. (28).

This quick derivation shows that for the kinematic situation when one of the final state gluons is emitted along the direction of an incoming quark, one can indeed combine the subtraction terms and the integrated subtraction terms computed in Ref. [30] with the phase-space parametrization Eq. (10). We have checked that the same holds for all other limits that are relevant for the NLO and NNLO computations. Apart from a more flexible parametrization, this result also provides a non-trivial check on the robustness of the subtraction procedure of Ref. [29] and allows us to use the subtraction terms derived in Ref. [30] without modification.

Finally, an important benefit of the phase-space parametrization described in this section is that both fully-resolved matrix elements and subtraction counterterms are always calculated in the same frame, without the need for longitudinal boosts. We find that this significantly improves the efficiency of the Monte-Carlo integration of the most complicated subtraction counterterms.

III. NNLO CORRECTIONS TO HIGGS PRODUCTION IN WBF

In this section we present results for fiducial cross sections and kinematic distributions for Higgs production in WBF. We begin in Section III A by treating the Higgs boson as a stable particle. This is important both for validating our results against previous calculations [17, 18] and as a reference for the case of the decaying Higgs boson which we study later. In the following subsections, we consider two phenomenologically important Higgs decay modes, namely $H \to b\bar{b}$ in Section III B and $H \to WW^* \to \ell^-\bar{\nu}\ell^+\nu$ in Section III C, and explore the

extent to which additional kinematic cuts applied to the decay products of the Higgs boson modify the NNLO QCD corrections.

For all phenomenological results reported in this paper, we use a baseline setup which is very similar (though not identical) to the one of Ref. [17]. We set the Higgs boson mass to $M_H = 125$ GeV, its width to $\Gamma_H = 4.165$ MeV, the vector boson masses to $M_W = 80.398$ GeV and $M_Z = 91.1876$ GeV, and their widths to $\Gamma_W = 2.105$ GeV and $\Gamma_Z = 2.4952$ GeV. We use the Fermi constant $G_F = 1.16639 \times 10^{-5}$ GeV^{-2}, and approximate the CKM matrix by an identity matrix. We employ the NNPDF31-nnlo-as-118 parton distribution functions [43] and use them for all calculations reported in this paper, irrespective of the perturbative order. We also use the value of the $\overline{\text{MS}}$ strong coupling constant $\alpha_s(M_Z) = 0.118$ as provided by the PDF set. The evolution of parton distribution functions and the strong coupling constant is obtained from LHAPDF [44]. We employ dynamical renormalization and factorization scales; their central values are set to [17]

$$\mu_0 = \sqrt{\frac{m_H}{2}\sqrt{\frac{m_H^2}{4} + p_{\perp,H}^2}}. \tag{29}$$

We consider proton-proton collisions with center-of-mass energy of 13 TeV, and define the WBF fiducial cross section in the following way. We reconstruct jets using the inclusive anti-$k_\perp$ algorithm [45] with $R = 0.4$. We then consider the list $J = \{j_i\}$ of jets satisfying $p_\perp \geq 25$ GeV, $|y| \leq 4.5$, and impose the following constraints. For each event, we require that J contains at least two jets. Furthermore, the two leading-$p_\perp$ jets in J should be separated by a large rapidity interval $|y_{j_1} - y_{j_2}| \geq 4.5$, and their invariant mass should be larger than 600 GeV. They should also be in different hemispheres in the laboratory frame; to enforce this, we require that the product of their rapidities is negative, $y_{j_1} y_{j_2} \leq 0$.

Before presenting our results, we briefly discuss the checks that we have performed on our calculation. For stable Higgs, we have first checked the inclusive cross section against a customized version of the proVBFH-inclusive code [46], which is based on the calculations of Refs. [16, 17] and on Ref. [47]. We have modified the original program to be able to compare individual contributions separately and we have found agreement with the corresponding results obtained from our calculation. Moving to fiducial results, we note that although our setup is very similar to the one in Ref. [17], it is not identical. In particular, we use updated parton distribution functions and a slightly different jet selection procedure. Because of this,

the results presented here cannot be directly compared with those of Ref. [17]. We have, however, produced a set of results with the setup of Ref. [17], and found agreement with the fiducial cross-sections reported there at the level of few per-mille or better. We have also compared differential distributions, and also in this case found good agreement within the numerical precision of the calculations. For the $H \to b\bar{b}$ and $H \to WW^* \to 4l$ results, we have compared our implementation against `MCFM` version 10 [48–51] at NLO and LO, respectively, and found perfect agreement.

A. Stable Higgs boson

In this section we present the fiducial cross sections for the production of a stable Higgs boson in WBF at NNLO in QCD. Analogous results have been already presented in Refs. [17, 18]. There are two reasons for us to repeat these computations. First, it allows us to validate our calculation. To this end, as we have mentioned already, we have performed an extensive comparison with the results of Ref. [17] for both inclusive and fiducial cross sections, and found agreement at the per-mille level or better in all cases. We also find excellent agreement with higher-order corrections to kinematic distributions presented in that reference. A second reason to consider WBF production with a stable Higgs boson is that it provides a benchmark against which to compare the results obtained by considering the decays of the Higgs boson that are discussed later.

We first report fiducial cross sections at various orders of QCD perturbation theory. Using the setup described above, we obtain

$$\sigma_{\mathrm{LO}} = 971^{-61}_{+69} \text{ fb}, \quad \sigma_{\mathrm{NLO}} = 890^{+8}_{-18} \text{ fb}, \qquad \sigma_{\mathrm{NNLO}} = 859^{+8}_{-10} \text{ fb}. \tag{30}$$

The central values of fiducial cross sections are computed with the renormalization and factorization scales of Eq. (29) and uncertainties are obtained by varying this scale by a factor of two in both directions. In Eq. (30) and throughout this paper, the sub- and super-scripts indicate the results computed with $\mu = \mu_0/2$ and $\mu = 2\mu_0$, respectively.

Results for cross sections show a familiar pattern [17, 18] – NLO and NNLO QCD corrections to fiducial cross sections are relatively small; they decrease the previous order cross section by about 8 and 3.5 percent, respectively. The uncertainty of σ_{NNLO} as estimated from scale
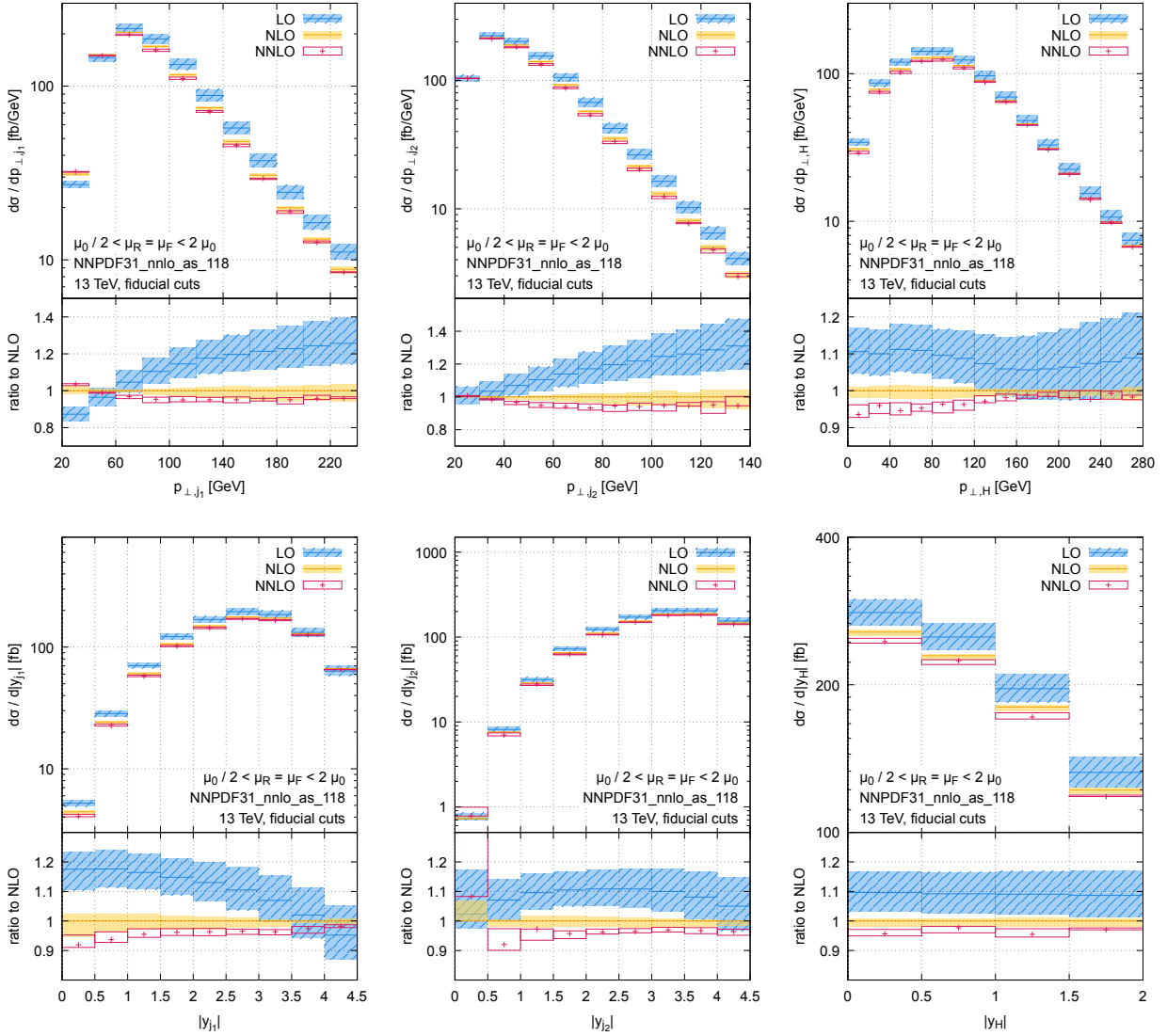
15

Figure 2. Transverse momenta (upper row) and rapidity (lower row) distributions for the leading (left) and subleading (middle) jets as well as the Higgs boson (right). For each plot, the upper pane displays the LO (hashed blue), NLO (solid yellow) and NNLO (red boxes) QCD predictions. The lower pane shows the ratio with respect to the NLO result at central scale. The lines indicate the central renormalization and factorization scale choice, and the bands indicate the envelope of the results at different scales. See text for details.

variation is about a percent, only marginally smaller than the NLO one. Although we do not show inclusive results here, we note that NNLO corrections to the inclusive WBF cross section are about one percent and, therefore, are significantly smaller than corrections to the fiducial cross section. This is not surprising, since WBF fiducial cuts induce a sensitivity of

theoretical predictions to the non-trivial jet dynamics present in this process, see e.g. the discussion in Ref. [52].

We now present results for kinematic distributions. In Fig. 2 NNLO QCD results for the transverse momentum and the rapidity distributions of the leading and subleading jets, as well as the Higgs boson, are shown. The upper panes in plots in Fig. 2 display LO, NLO and NNLO QCD predictions in hashed blue, yellow, and red boxes, respectively. The lines indicate the central renormalization and factorization scale choice $\mu = \mu_0$ in Eq. (29), and the bands indicate the envelope of the results at scales $\mu \in \{\mu_0/2, \mu_0, 2\mu_0\}$. For transverse momenta distributions, we observe that in all cases the NNLO/NLO bin-by-bin K-factors are reasonably flat, at variance to the NLO/LO ones that exhibit strong dependencies on transverse momenta of the leading and subleading jets. For the Higgs rapidity distribution, both NLO/LO and NNLO/NLO K-factors are approximately flat in the bulk of the distribution and consistent with the corrections to fiducial cross sections reported in Eq. (30). For the jets rapidity distributions, the NLO/LO K-factors have a non-trivial shape (especially in the leading jet case) but the NNLO/NLO ones are fairly flat.

The identification of the weak boson fusion process exploits kinematic features of the two leading jets. It is therefore interesting to check how kinematic distributions that involve them get modified in higher orders of perturbation theory. In Fig. 3 we display the invariant mass distribution of the two leading jets, their rapidity difference $\Delta y_{j_1 j_2} = |y_{j_1} - y_{j_2}|$ and the relative azimuthal angle $|\phi_{j_1} - \phi_{j_2}|$ distributions, as well as the distribution of the distance between the two jets in the transverse plane $\Delta R_{j_1, j_2} = \sqrt{(y_{j_1} - y_{j_2})^2 + (\phi_{j_1} - \phi_{j_2})^2}$. The distribution of the dijet invariant mass and the $\Delta\phi_{j_1 j_2}$ distribution exhibit rather flat K-factors, both at NLO and at NNLO. By contrast, the NLO/LO K-factors for the rapidity difference and $\Delta R_{j_1 j_2}$ show stronger dependencies on the corresponding variables, but they stabilize at NNLO.

In summary, we find that although NLO QCD corrections can have an important impact on the shapes of differential distributions of Higgs production in WBF, the impact of NNLO corrections is much milder and it is captured by an overall K-factor to a reasonable approximation. However, the NNLO distributions often lie outside of the NLO scale variation bands, although distances between the NLO and NNLO bands are small. We note that this is also the case for the fiducial cross sections shown in Eq. (30).
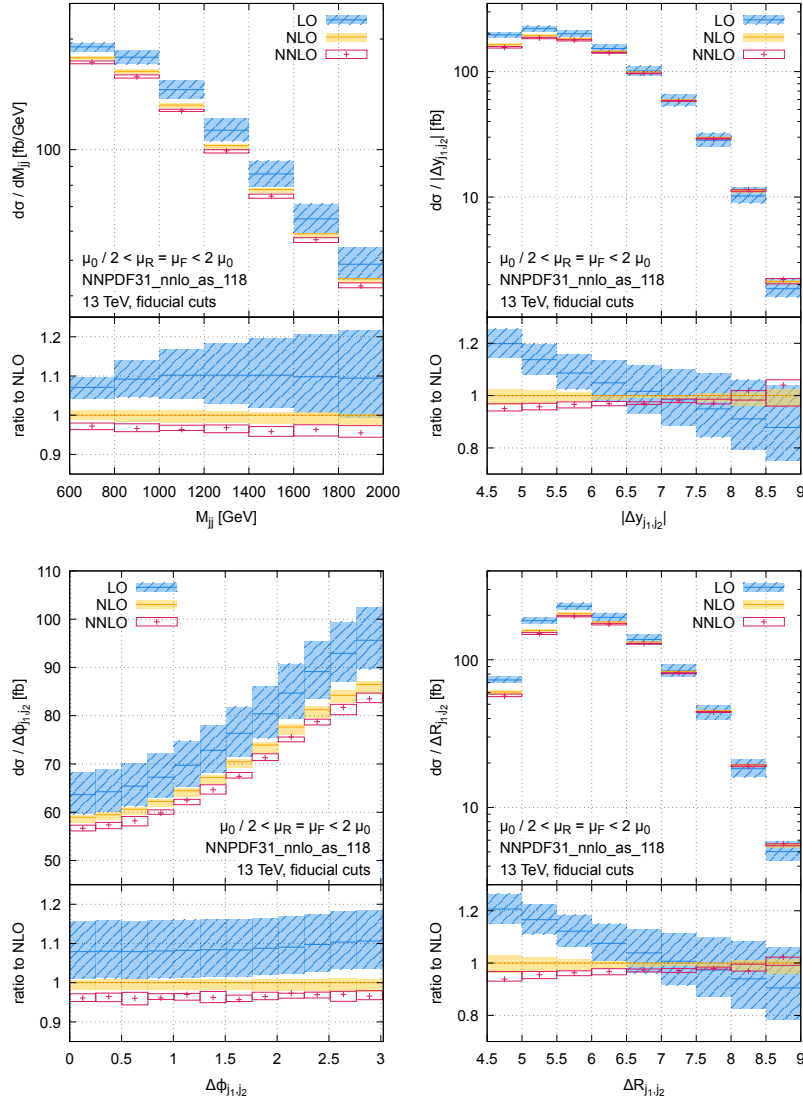
Figure 3. Kinematic distributions of observables that involve the two leading jets for a stable Higgs. Top row: dijet invariant mass distribution (left) and rapidity separation (right). Bottom row: azimuthal (left) and ΔR (right) separations. See text for details.

B. Results for $H \to b\bar{b}$

In this section we study NNLO QCD corrections to Higgs production in WBF, taking into account Higgs boson decays to a $b\bar{b}$-pair. The radiative corrections acquire a dependence on the kinematics of Higgs boson decay products because their four-momenta are used to define the selection criteria, as we now explain.

In case of $H \to b\bar{b}$ decays, the Higgs boson is identified and reconstructed through an ob-

servation of two b-jets. Since the b-quarks from Higgs boson decays sometimes get clustered with other final state partons and since the Higgs boson momentum is then identified with the total momentum of two b-jets, it is not guaranteed that the momentum of the $b\bar{b}$ dijet system equals the momentum of the Higgs boson. In principle, to reconstruct b-jets properly, we need to carefully track flavor in the production process since initial-state partons include b quarks that propagate into the final state, leading to b jets that originate in the production process. Also, starting from NNLO final state splittings $g^* \to b\bar{b}$ generate additional $b\bar{b}$ pairs in the final state. However, it can be checked that both of these effects are rather small for WBF. Indeed, at NLO b-quarks in the final state contribute about one percent of the cross section. Since we do not expect this result to change significantly at NNLO, we decided to treat all quarks coming from the production stage as flavorless and not account for them when determining b-tags of jets.

As a second approximation, we note that in this paper we consider Higgs boson decays to massless $b\bar{b}$ pairs only at leading order in QCD. It will be desirable to extend this calculation and include higher order QCD corrections to Higgs decay as well. We leave this for future work but we note that the computation reported in this paper, that describes an interplay of NNLO QCD corrections to the production stage with leading order decays, is an important step towards this goal.

To account for Higgs boson decays, we make use of the fact that Higgs bosons are narrow scalar particles, so that their production and decay subprocesses are not correlated and can be considered separately. For this reason, we generate kinematics of final state particles in the $H \to b\bar{b}$ process in the Higgs boson rest frame independently of the production stage. Then, we use high-quality importance-sampling grids that describe stable Higgs production in weak boson fusion to generate properly distributed events with a given Higgs four-momentum. For each production point, we consider $\mathcal{O}(10)$ randomly generated decay events. We then adjust the weight of each event to account for the $H \to b\bar{b}$ branching ratio, which we take to be $\mathrm{Br}(H \to b\bar{b}) = 0.5824$ [9]. Finally, we boost the momenta of b-quarks back to the laboratory frame, use them to reconstruct jets and check if final state objects pass the selection criteria that we now describe.

Similar to the case of a stable Higgs boson, we reconstruct jets using the anti-k_t algorithm and b-tag them according to whether they contain a single b-quark or not. As we have

already said, we work in an approximation where we have a single $b\bar{b}$ pair coming from the Higgs so this procedure is infra-red safe. In addition to the kinematic cuts described in the previous section, we loosely follow Ref. [22] and require that an event contains at least two b-jets with $p_{\perp j_b} \geq 65$ GeV and with their rapidities confined to the interval $|y_{j_b(j_{\bar{b}})}| \leq 2.5$. The WBF cuts described in the preceding section are applied exclusively to non b-jets.

We turn to the presentation of our results. We first report values of fiducial cross sections. Using the setup described above, we obtain

$$\sigma_{\mathrm{LO}}^{b\bar{b}} = 75.9_{+6.5}^{-5.6} \text{ fb}, \qquad \sigma_{\mathrm{NLO}}^{b\bar{b}} = 70.9_{-1.2}^{+0.2} \text{ fb}, \qquad \sigma_{\mathrm{NNLO}}^{b\bar{b}} = 69.4_{-0.2}^{+0.5} \text{ fb}. \tag{31}$$

The central values correspond to the scale μ_0 shown in Eq. (29); the subscript and superscript show the cross section at $\mu = \mu_0/2$ and at $\mu = 2\mu_0$ respectively.

It is interesting to compare the size of fiducial NLO and NNLO QCD corrections for stable and decaying Higgs boson. Using Eqs. (30,31) we find (for $\mu = \mu_0$)

$$\begin{aligned}
\frac{\sigma_{\mathrm{NLO}}^{H}}{\sigma_{\mathrm{LO}}^{H}} &= 0.917(1), & \frac{\sigma_{\mathrm{NLO}}^{b\bar{b}}}{\sigma_{\mathrm{LO}}^{b\bar{b}}} &= 0.934(1), \\
\frac{\sigma_{\mathrm{NNLO}}^{H}}{\sigma_{\mathrm{LO}}^{H}} &= 0.885(1), & \frac{\sigma_{\mathrm{NNLO}}^{b\bar{b}}}{\sigma_{\mathrm{LO}}^{b\bar{b}}} &= 0.914(2),
\end{aligned} \tag{32}$$

where the Monte Carlo integration error is shown in parentheses. Eq. (32) shows that for stable Higgs boson the NNLO QCD cross section is smaller than the leading order cross section by about -11.5 percent whereas for $b\bar{b}$ final state the NNLO QCD cross section is smaller than the leading order cross section by about -8.5 percent. This 3 percent difference is clearly not a large one; however, it is of the same order as the NNLO QCD corrections themselves. It is also interesting that the difference between the two scenarios is slightly more pronounced at NNLO than at NLO, where the corrections decrease the LO fiducial cross section by about -8 percent for a stable Higgs and by about -6.5 percent when we allow for Higgs decays.

As we now explain, this difference is largely caused by the cuts on the transverse momenta of the b-tagged jets, which make the Higgs $p_\perp$ spectrum harder. This is illustrated in Fig. 4, where we show the transverse momentum and rapidity distributions of the $b\bar{b}$-dijet system that should be identified with the Higgs boson. By comparing with the analogous plots in Fig. 2, we see that the differential K-factors are rather similar, but now the reconstructed
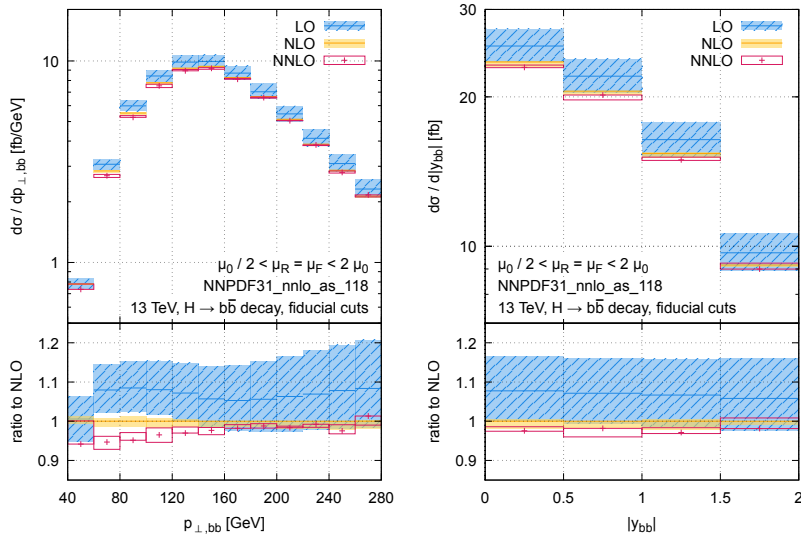
Figure 4. Transverse momentum (left) and rapidity (right) distribution of the reconstructed Higgs boson in the $H \to b\bar{b}$ decay channel. See text for details.

Higgs transverse momentum peaks around 150 GeV instead of 100 GeV which is the case if no cuts on the b-jets are imposed, see Fig. 2. This observation explains the difference in K-factors. Indeed, if we impose the requirement $p_{\perp,H} \geq 150$ GeV on our results for the stable Higgs, we find that the ratio of NNLO to LO fiducial cross sections becomes about 0.91, quite similar to what we find by considering $H \to b\bar{b}$ decays and imposing cuts on b-jets. Hence, our results show that a decent estimate of the fiducial K-factor in this case can be obtained by considering stable Higgs boson and computing the K-factor with the cut $p_{\perp,H} \geq 150$ GeV.[5]

Compared to the results that do not include decays of the Higgs boson presented in the previous section, it is interesting to note that in the $H \to b\bar{b}$ fiducial region the NNLO QCD cross section overlaps with the scale-uncertainty band of the NLO QCD cross section. Furthermore, the relative scale variation of the NNLO result is smaller by about a factor two compared to the stable Higgs result. These features are also explained by the fact that, when $H \to b\bar{b}$ decays are considered, the Higgs boson typically has larger transverse momentum and, as follows from Fig. 2, at higher $p_\perp$ the NNLO result tends to get closer to the NLO one and lies within the NLO scale variation band.

We continue with the discussion of kinematic distributions for observables that involve the

---

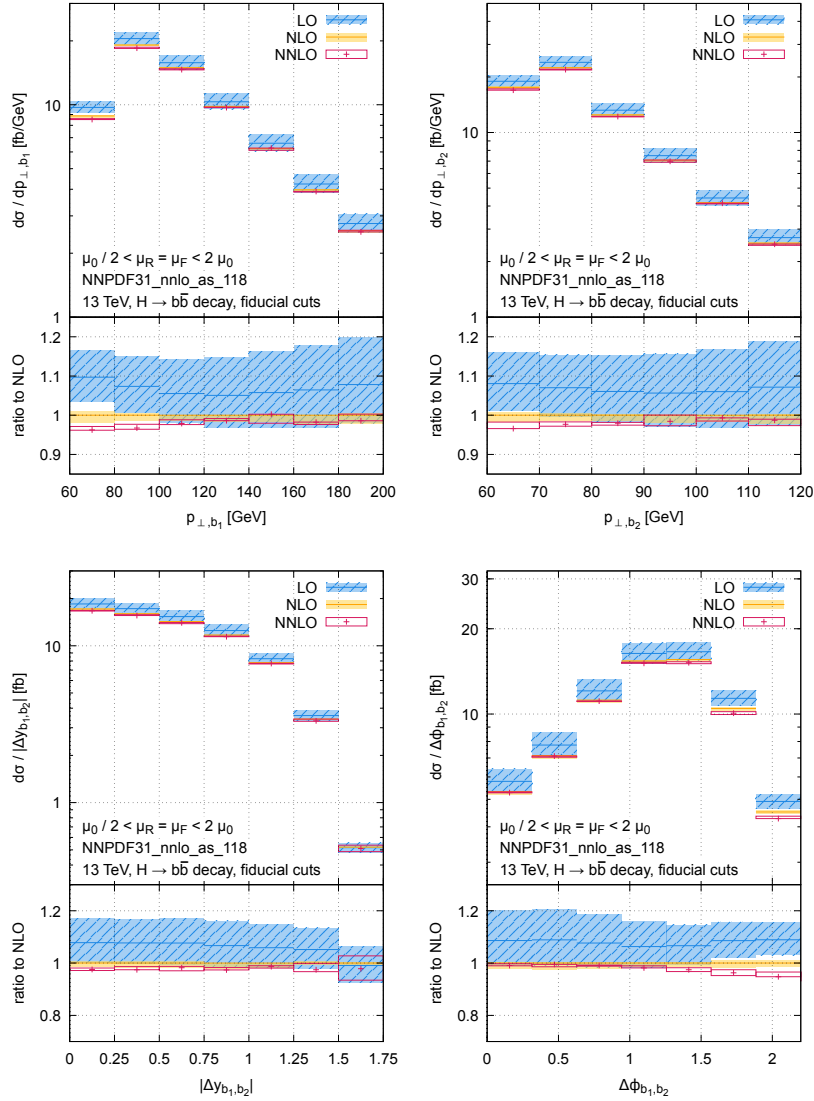[5] We note that it is customary to impose a $p_{\perp,b\bar{b}} \geq 150$ GeV cut in this channel [22].

Figure 5. Various kinematic distributions that involve b-jets from Higgs boson decays. Top row: leading (left) and subleading (right) b-jet transverse momentum distribution. Bottom row: rapidity (left) and azimuthal (right) separation between the two leading b-jets. See text for details.

reconstructed b-jets. They are shown in Fig. 5, where we plot the transverse momentum distribution of the leading-$p_\perp$ (b_1) and subleading-$p_\perp$ (b_2) reconstructed b-jets, as well as their rapidity and azimuthal separation. We find that in the bulk of the distribution the K-factors are rather flat, with the possible exception of the leading-$p_\perp$ b-jet at NLO. Similar to the stable Higgs case, the NNLO/NLO K-factor is flatter than the NLO/LO one.

As we mentioned earlier, b-quarks from Higgs decays may get recombined with some of the
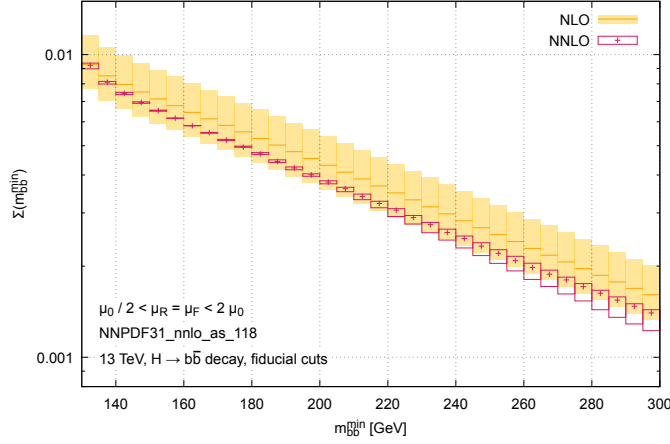
Figure 6. Fraction of events Σ for which the reconstructed Higgs mass is larger than the true Higgs mass. See text for details.

partons in the production process. If this happens, the reconstructed Higgs boson will have a non-trivial invariant mass distribution, even if the Higgs boson is on-shell. Since the Higgs boson is produced centrally in WBF, while QCD radiation is mostly collinear to leading jets, we expect this to happen very rarely. This expectation is confirmed by Fig. 6, where we show the fraction of events Σ where the reconstructed Higgs mass $m_{b\bar{b}}$ is larger than a given value $m_{b\bar{b}}^{\min}$, i.e.

$$\Sigma(m_{b\bar{b}}^{\min}) = \frac{1}{\sigma} \int\limits_{m_{b\bar{b}}^{\min}}^{\infty} \mathrm{d}m_{b\bar{b}} \frac{\mathrm{d}\sigma}{\mathrm{d}m_{b\bar{b}}}. \tag{33}$$

In Fig. 6, we normalize the (N)NLO invariant mass distribution to the corresponding fiducial cross section, integrated over the invariant mass. We see that indeed only about 1% of the events have a reconstructed mass $m_{b\bar{b}}$ that exceeds the Higgs mass $M_H = 125$ GeV.

C. Results for $H \to WW^* \to \ell^- \bar{\nu} \ell^+ \nu$

We now turn to Higgs production in weak boson fusion followed by the Higgs decay to two W bosons which decay leptonically, $H \to WW^* \to e\bar{\nu}_e \mu \nu_\mu$. Although this is a higher multiplicity final state than considered in the previous section, from a conceptual point of view it is simpler in the sense that the Higgs decay products are not clustered with any of the QCD partons. As done for $H \to b\bar{b}$ in the previous section, we account for the $H \to WW^* \to e\bar{\nu}_e \mu \nu_\mu$ decay by generating kinematics of the decay products in the Higgs

rest frame and boosting the decay products into the lab frame. Compared to the $H \to b\bar{b}$ case considered earlier, the decay phase space is now much larger. To properly sample it, we then consider $\mathcal{O}(100)$ randomly selected decay events per production point, instead of $\mathcal{O}(10)$ events that we used for $H \to b\bar{b}$. In general, we note that, compared to $H \to b\bar{b}$, it is much harder to efficiently sample the phase space in the four-lepton case.

We now define the fiducial region for this decay channel. In addition to the cuts described in Section III A, we impose cuts on the particles arising from the Higgs decay following Ref. [24]. We require that the leading charged lepton has transverse momentum $p_{\perp,l_1} \geq 25$ GeV while the subleading charged lepton should have transverse momentum $p_{\perp,l_2} \geq 13$ GeV. The invariant mass of the charged-leptons system should satisfy $m_{l_1 l_2} \geq 12$ GeV, its transverse momentum $p_\perp^{l_1 l_2}$ should exceed 30 GeV, the missing transverse momentum should be larger than 20 GeV and the rapidities of the charged leptons should be between the rapidities of the two hardest jets. We note that this cut correlates the production and decay stages and, given the forward nature of leading jets, it selects Higgs bosons produced in the central rapidity region. Finally, we require the transverse mass, defined as

$$
m_T = \sqrt{2 p_\perp^{l_1 l_2} p_\perp^{\text{miss}} \left(1 - \cos \Delta\phi_{l_1 l_2, \vec{p}_\perp^{\text{miss}}} \right)},
\tag{34}
$$

to satisfy 60 GeV $\leq m_T \leq$ 125 GeV. In Eq. (34), $p_T^{l_1 l_2}$ and p_T^{miss} are the transverse momenta of the charged-leptons system and the missing transverse momentum, respectively, while $\Delta\phi_{l_1 l_2, \vec{p}_T^{\text{miss}}}$ is the azimuthal angle between the transverse momenta of the charged-leptons and two-neutrinos systems.

Computing fiducial cross sections, we obtain

$$
\sigma_{\text{LO}}^{e\bar{\nu}_e \bar{\mu}\nu_\mu} = 0.719_{+0.051}^{-0.045} \text{ fb}, \qquad \sigma_{\text{NLO}}^{e\bar{\nu}_e \bar{\mu}\nu_\mu} = 0.662_{-0.012}^{+0.005} \text{ fb}, \qquad \sigma_{\text{NNLO}}^{e\bar{\nu}_e \bar{\mu}\nu_\mu} = 0.632_{-0.008}^{+0.008} \text{ fb}.
\tag{35}
$$

The pattern of the corrections is very similar to what we observed in Section III A for the stable Higgs case: the NLO corrections reduce the cross section by -8 percent and the NNLO corrections reduce it by additional -4.5 percent. The relative scale variation uncertainty is also similar to the stable Higgs case. These features can be understood since, in contrast to Section III B, we impose relatively mild cuts on the Higgs decay products which do not force the kinematics of the Higgs boson to differ significantly from the stable case. Indeed, we have checked that, in this fiducial region, the differential distributions of the Higgs and the jets are very similar to the corresponding results for the stable Higgs boson.
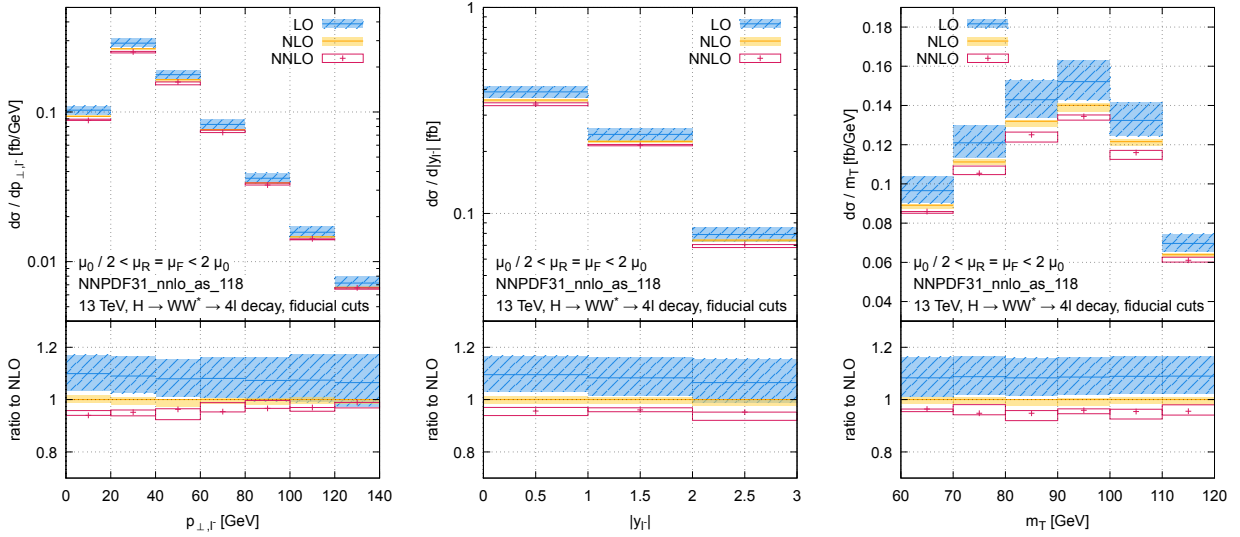
Figure 7. Various kinematic distributions that involve charged leptons from Higgs boson decays. From left to right: transverse momentum and rapidity distribution of the negatively charged lepton, and transverse mass of the charged-leptons system. See text for details.

In Fig. 7 we present results for selected kinematic distributions of the two charged leptons. We show the transverse momentum and rapidity of the negatively-charged lepton and the transverse mass defined in Eq. (34). We see that already at NLO the K-factors are rather flat and this remains true at NNLO. This is not surprising since in this case the only impact of radiative corrections comes from the interplay between jet and lepton cuts. As we mentioned earlier, the leptonic cuts that we employ are rather mild and do not severely affect the kinematics of the Higgs boson. In particular, the only cut that correlates jets and leptons is the requirement that the charged lepton rapidity should lie within the rapidities of the two hard jets. However, the tagging jets are mostly produced along the beam line, so this requirement is satisfied by most of the events.

In summary, our results show that in this channel the impact of Higgs decays on radiative corrections is milder. This happens because the kinematic features of the Higgs boson and of the jets remain unaffected by the fiducial cuts on leptons and, as a consequence, corrections to leptonic observables are rather flat and can be described to a very good approximation with a global K-factor corresponding to fiducial cross section for stable Higgs.

IV. CONCLUSIONS

In this paper, we presented a computation of NNLO QCD corrections to Higgs boson production in weak boson fusion using the nested soft-collinear subtraction scheme. We have used analytic formulas for the required NNLO integrated subtraction terms derived in Ref. [30]. We have shown that, although we employ a somewhat different phase-space parametrization for the current computation, the results derived in Ref. [30] remain applicable.

We have confirmed earlier results on NNLO QCD corrections to fully-differential Higgs boson production in weak boson fusion obtained in Refs. [17, 18]. We have also extended these results by incorporating decays of the Higgs boson into the calculation. We considered two Higgs decay modes that are important for WBF studies, namely $H \to b\bar{b}$ and $H \to WW^* \to 4$ leptons. We observed that in the $H \to b\bar{b}$ case the perturbative behavior of the fiducial cross section differs from the stable Higgs case. In particular, we found that, while the NLO/LO ratio is very similar for stable Higgs and for $H \to b\bar{b}$, the difference in the NNLO/LO ratio is comparable to the NNLO QCD corrections themselves.

We have argued that the main reason for this difference is that the cuts on the b-jets push the transverse momentum of the Higgs boson towards larger values, where NNLO corrections are small. If this effect is taken into account, the impact of radiative corrections in the stable-Higgs approximation and in the $H \to b\bar{b}$ decay channel become very similar. In both cases, shapes of NLO distributions are not significantly affected by NNLO corrections so that a rescaling of NLO distributions would provide a good approximation to the full result. We stress that this would *not* be the case if one were to use a NNLO/NLO K-factor computed in the standard WBF fiducial region, without an additional $p_{\perp,H} \gtrsim 150$ GeV cut.

In the $H \to WW^* \to 4l$ channel, typical selection cuts are milder and do not significantly affect the Higgs and jets kinematic distributions. Because of this, corrections to Higgs and leptonic observables are rather flat and can be well captured by an overall K-factor.

Our results could be extended in several directions. Most prominently, our $H \to b\bar{b}$ analysis is only approximate. Indeed, we did not consider radiative corrections to $H \to b\bar{b}$ decay. Given the non-trivial interplay between jets coming from the production stage and jets originated from the b-quarks from Higgs decays, it would be interesting to perform a *complete* NNLO analysis that accounts for corrections to both the production and decay stages of the WBF

26

process.

Furthermore, since radiative corrections to WBF in the fiducial region are impacted by a non-trivial jet dynamics, it is difficult to predict how potential Beyond the Standard Model effects would impact the radiative corrections. To study this point, one could, for example, repeat the NNLO QCD calculation within the Standard Model effective field theory framework, to investigate to which extent radiative corrections can mimic potential anomalous couplings effects if the latter are only predicted at low orders in QCD perturbation theory. We leave these interesting avenues of investigation for the future.

[1] G. Aad *et al.* (ATLAS), Phys. Rev. D **101**, 012002 (2020).

[2] A. M. Sirunyan *et al.* (CMS), Eur. Phys. J. C **79**, 421 (2019).

[3] G. Heinrich, Phys. Rept. **922**, 1 (2021).

[4] T. Plehn, D. L. Rainwater, and D. Zeppenfeld, Phys. Rev. Lett. **88**, 051801 (2002).

[5] G. Aad *et al.* (ATLAS), Eur. Phys. J. C **76**, 658 (2016).

[6] A. M. Sirunyan *et al.* (CMS), Phys. Rev. D **100**, 112002 (2019).

[7] G. Aad *et al.* (ATLAS), JHEP **01**, 172 (2016).

[8] A. M. Sirunyan *et al.* (CMS), Phys. Lett. B **793**, 520 (2019).

[9] D. de Florian *et al.* (LHC Higgs Cross Section Working Group), **2/2017** (2016), 10.23731/CYRM-2017-002.

[10] A. Buckley *et al.*, (2021), arXiv:2105.11399 [hep-ph].

[11] T. Han, G. Valencia, and S. Willenbrock, Phys. Rev. Lett. **69**, 3274 (1992).

[12] M. Ciccolini, A. Denner, and S. Dittmaier, Phys. Rev. Lett. **99**, 161803 (2007).

[13] M. Ciccolini, A. Denner, and S. Dittmaier, Phys. Rev. D **77**, 013002 (2008).

[14] T. Figy, C. Oleari, and D. Zeppenfeld, Phys. Rev. D **68**, 073005 (2003).

[15] P. Bolzoni, F. Maltoni, S.-O. Moch, and M. Zaro, Phys. Rev. Lett. **105**, 011801 (2010); Phys. Rev. D **85**, 035002 (2012).

[16] F. A. Dreyer and A. Karlberg, Phys. Rev. Lett. **117**, 072001 (2016).

[17] M. Cacciari, F. A. Dreyer, A. Karlberg, G. P. Salam, and G. Zanderighi, Phys. Rev. Lett. **115**, 082002 (2015), [Erratum: Phys.Rev.Lett. 120, 139901 (2018)].

[18] J. Cruz-Martinez, T. Gehrmann, E. W. N. Glover, and A. Huss, Phys. Lett. B **781**, 672 (2018).

[19] T. Liu, K. Melnikov, and A. A. Penin, Phys. Rev. Lett. **123**, 122002 (2019).

[20] F. A. Dreyer, A. Karlberg, and L. Tancredi, JHEP **10**, 131 (2020).

[21] D. Maître, J. Phys. Conf. Ser. **1525**, 012014 (2020).

[22] G. Aad *et al.* (ATLAS), Eur. Phys. J. C **81**, 537 (2021).

[23] G. Aad *et al.* (ATLAS), Phys. Rev. D **92**, 012006 (2015); M. Aaboud *et al.* (ATLAS), JHEP **11**, 112 (2016); Phys. Rev. D **98**, 052003 (2018); Phys. Lett. B **789**, 508 (2019); G. Aad *et al.* (ATLAS), JHEP **03**, 268 (2021).

[24] A. M. Sirunyan *et al.* (CMS), Phys. Lett. B **791**, 96 (2019).

[25] V. Khachatryan *et al.* (CMS), Phys. Rev. D **92**, 032008 (2015); A. M. Sirunyan *et al.* (CMS), JHEP **03**, 003 (2021).

[26] W. Bernreuther, L. Chen, and Z.-G. Si, JHEP **07**, 159 (2018).

[27] A. Behring, W. Bizoń, F. Caola, K. Melnikov, and R. Röntsch, Phys. Rev. D **101**, 114012 (2020).

[28] A. Gehrmann-De Ridder, T. Gehrmann, and E. W. N. Glover, JHEP **09**, 056 (2005); Phys. Lett. B **612**, 36 (2005); Phys. Lett. B **612**, 49 (2005); A. Daleo, T. Gehrmann, and D. Maitre, JHEP **04**, 016 (2007); A. Daleo, A. Gehrmann-De Ridder, T. Gehrmann, and G. Luisoni, JHEP **01**, 118 (2010); R. Boughezal, A. Gehrmann-De Ridder, and M. Ritzmann, JHEP **02**, 098 (2011); T. Gehrmann and P. F. Monni, JHEP **12**, 049 (2011); A. Gehrmann-De Ridder, T. Gehrmann, and M. Ritzmann, JHEP **10**, 047 (2012); J. Currie, E. W. N. Glover, and S. Wells, JHEP **04**, 066 (2013).

[29] F. Caola, K. Melnikov, and R. Röntsch, Eur. Phys. J. C **77**, 248 (2017).

[30] K. Asteriadis, F. Caola, K. Melnikov, and R. Röntsch, Eur. Phys. J. C **80**, 8 (2020).

[31] S. Catani, Phys. Lett. B **427**, 161 (1998).

[32] T. Becher and M. Neubert, Phys. Rev. Lett. **102**, 162001 (2009), [Erratum: Phys.Rev.Lett. 111, 199905 (2013)]; JHEP **06**, 081 (2009), [Erratum: JHEP 11, 024 (2013)].

[33] M. Czakon, Phys. Lett. B **693**, 259 (2010); Nucl. Phys. B **849**, 250 (2011); M. Czakon and D. Heymes, Nucl. Phys. B **890**, 152 (2014); R. Boughezal, K. Melnikov, and F. Petriello, Phys. Rev. D **85**, 034025 (2012).

[34] S. Catani and M. Grazzini, Phys. Rev. Lett. **98**, 222002 (2007); M. Grazzini, JHEP **02**, 043 (2008).

[35] J. Gaunt, M. Stahlhofen, F. J. Tackmann, and J. R. Walsh, JHEP **09**, 058 (2015); R. Boughezal, C. Focke, X. Liu, and F. Petriello, Phys. Rev. Lett. **115**, 062002 (2015); J. M. Campbell, R. K. Ellis, R. Mondini, and C. Williams, Eur. Phys. J. C **78**, 234 (2018).

[36] V. Del Duca, C. Duhr, A. Kardos, G. Somogyi, and Z. Trócsányi, Phys. Rev. Lett. **117**, 152004 (2016); V. Del Duca, C. Duhr, A. Kardos, G. Somogyi, Z. Szőr, Z. Trócsányi, and Z. Tulipánt, Phys. Rev. D **94**, 074019 (2016).

[37] L. Magnea, E. Maina, G. Pelliccioli, C. Signorile-Signorile, P. Torrielli, and S. Uccirati, JHEP **12**, 107 (2018), [Erratum: JHEP 06, 013 (2019)]; JHEP **12**, 062 (2018).

[38] F. Herzog, JHEP **08**, 006 (2018).

[39] F. Caola, M. Delto, H. Frellesvig, and K. Melnikov, Eur. Phys. J. C **78**, 687 (2018).

[40] S. Catani and M. Grazzini, Nucl. Phys. B **570**, 287 (2000).

[41] S. Frixione, Z. Kunszt, and A. Signer, Nucl. Phys. B **467**, 399 (1996); S. Frixione, Nucl. Phys. B **507**, 295 (1997).

[42] M. Delto and K. Melnikov, JHEP **05**, 148 (2019).

[43] R. D. Ball *et al.* (NNPDF), Eur. Phys. J. C **77**, 663 (2017).

[44] A. Buckley, J. Ferrando, S. Lloyd, K. Nordström, B. Page, M. Rüfenacht, M. Schönherr, and G. Watt, Eur. Phys. J. C **75**, 132 (2015).

[45] M. Cacciari, G. P. Salam, and G. Soyez, JHEP **04**, 063 (2008).

[46] https://provbfh.hepforge.org.

[47] G. P. Salam and J. Rojo, Comput. Phys. Commun. **180**, 120 (2009).

[48] https://mcfm.fnal.gov.

[49] J. M. Campbell and R. K. Ellis, Phys. Rev. D **60**, 113006 (1999).

[50] J. M. Campbell, R. K. Ellis, and W. T. Giele, Eur. Phys. J. C **75**, 246 (2015).

[51] J. Campbell and T. Neumann, JHEP **12**, 034 (2019).

[52] M. Rauch and D. Zeppenfeld, Phys. Rev. D **95**, 114015 (2017).